



*Research article*

## **Novel laser tracking measurement system based on the position sensitive detector**

**Jin Liu<sup>1</sup>, Fan Zhang<sup>1</sup>, Aleksey Kudreyko<sup>2</sup>, Wenjia Ren<sup>1</sup> and Haima Yang<sup>3,\*</sup>**

<sup>1</sup> School of Electronic and Electrical Engineering, Shanghai University of Engineering Science, Shanghai 201620, China

<sup>2</sup> Department of Medical Physics and informatics, Bashkir State Medical University, Lenina st. 3, 450008 Ufa, Russia

<sup>3</sup> School of Optical-Electrical and Computer Engineering, University of Shanghai for Science and Technology, Shanghai 200093, China

\* **Correspondence:** Email: [snowyhm@sina.com](mailto:snowyhm@sina.com).

**Abstract:** The rapid development of modern industrial technology has led to the increase of machinery precision. Laser tracking measurement systems represent a novel type of coordinate measurement method, which was developed on the basis of metrology. In this paper, we aim to define a single-station 3D coordinate rotating laser tracking measurement system based on the principle of the space coordinate method. In view of the current architecture and optical path of the system, we establish the ideal mathematical model of the system and derive the coordinate expression for arbitrary measured points in the measurement space. The output response of the photoelectric position detector to the rotating laser and the linearity of the position signal in the detection circuit have been detected via a concrete experiment. A laser tracking system was used to track the target mirror mounted on the coordinate measuring machine measuring spindle. It is shown that stable tracking is possible during the 3D movement of a cat's eye retroreflector if its velocity is 0.2 m/s and the distance to the moving object is 1–2 m. The corresponding velocity of the object must be 0.4 m/s. Our system provides a feasible implementation method for the tracking of the moving target space position.

**Keywords:** photoelectric position sensor; spatial coordinate method; rotating laser; coordinate measurement; track

---

## 1. Introduction

There exist many measurement requirements for geometric features, which are hardly satisfied by traditional measurement methods. For example, measurements of three-dimensional objects are achieved through a series of iterations.

The accuracy requirements for the measurement have increased from micron to nanometer, and the measured size range has also expanded from several micrometers to large dimensions of tens of meters or even hundreds of meters. The requirements for the suitability of measurement systems are increasing. The measurement of various geometric parameters and on-site online measurements have become major developmental trends in modern quality control engineering and other measurement control fields. The requirements for automation, intelligence, networking and measurement speed of measurement systems are also increasing [1–4].

Position-sensitive detectors (PSDs) use the photoelectric effect to detect the relative position of spots on the photosensitive surface of the detector. Compared with the traditional charge coupled device sensor, PSDs have the advantages of a wide spectral response range, high resolution, high positioning accuracy and quick computation. It is widely used in laser collimation, laser tracking, spot position detection and other fields [5–8]. At present, the way to achieve laser tracking measurement is mainly to use laser trackers, on the basis of traditional laser interferometer ranging measurement, tracking mirrors are introduced to track spatially moving targets. In order to achieve good tracking characteristics for the laser beam, one must improve the aiming accuracy of the tracking system; the rotating laser tracking system based on the space coordinate method is designed in this paper [9–11]. The output response of the photoelectric PSD to the rotating laser and the linearity of the sensing position signal of the detection circuit are analyzed. Engineering-based three-dimensional coordinate measurement technology is mainly used in the acceptance measurement of the geometric parameters of parts, active measurements in the production process, tracking measurements for the moving target space position, assembly and debugging of large engineering structures, data acquisition of reverse engineering and engineering experimental analysis [12–15]. It is one of the most significant technologies.

## 2. Three-dimensional coordinate measurements

The coordinate measurement system based on the space coordinate method determines the three-dimensional coordinates of the measured point by measuring a length value and two angle values; the mathematical model principle is shown in Figure 1.

The three-dimensional coordinates of the  $P_i$  point can be determined by measuring the yaw angle  $\phi_i$ , the pitch angle  $\theta_i$  and the length  $L_i$ . The space coordinate method-based laser tracking measurement system does not need to calibrate the system with external standard parts, which is its main advantage. However, the point coordinates are still determined by the angle measurement method in two directions perpendicular to the beam (i.e., the line connecting the measured base point and the measured point). The measurement error increases with the distance between the measurement base point and the measured point linearly [16,17].

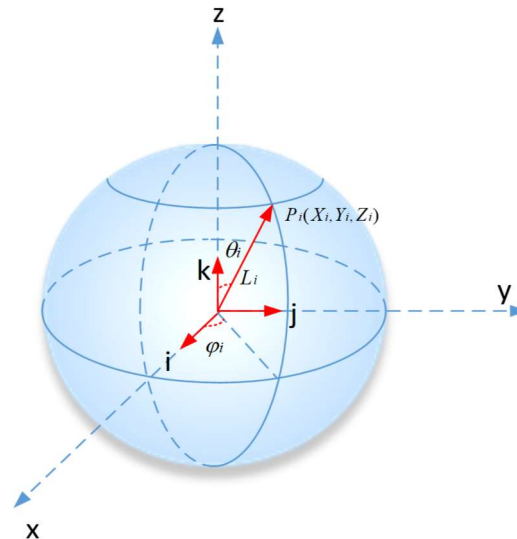


**Figure 1.** Schematic representation of the coordinate measurement.

### 2.1. Systematic mathematical modeling

Let us consider the ideal case of the laser tracking measurement system combined with the actual architecture (see Figure 2). Here, the z axis is appointed as the laser beam projection direction, the y-axis direction is outward perpendicular to the paper surface and x-axis direction is determined according to the right-hand rule. The following coordinate systems have been established: the laser coordinate system  $\{O_{LH} : X_{LH}, Y_{LH}, Z_{LH}\}$ , reflector coordinate system  $\{O_R : X_R, Y_R, Z_R\}$ , tracking mirror coordinate system  $\{O_{TM} : X_{TM}, Y_{TM}, Z_{TM}\}$  and world reference coordinate system  $\{O_W : X_W, Y_W, Z_W\}$ .

In addition, the target mirror  $P_i$  spherical coordinate system  $\{O_P : L_i, \varphi_i, \theta_i\}$  has also been established, and its origin  $O_P$  was set at the measurement base point  $O_B$  (at this time, the two-axis rotation base point  $O$ , the measurement base point  $O_B$  and the reflection base point  $O_{TM}$  coincide at three points). The specific coordinate axis direction setting is shown in Figure 1. In the laser tracking measurement system based on the space coordinate method, in order to establish the complete and accurate mathematical model shown in Figure 2, the following two factors must be considered.

First, the laser tracking measurement system can only measure the relative distance of the target mirror. In the measurement, a known point must be used as a reference point. (If the absolute distance  $L_i$  of the base point  $O_B$  to the space point  $P_i$  needs to be measured, a known reference distance  $LB$  must be given for system calibration.)

Second, the intersection of the pitch rotation axis  $Lx$  and the yaw rotation axis  $Ly$  is  $O$ . The reflection base point  $O_{TM}$  of the tracking mirror in the laser tracking measurement system and the measurement base point  $O_B$  of the system were both set at the  $O$  point. Therefore, both the reflection base point  $O_{TM}$  and the measurement base point  $O_B$  coincides at the point  $O$ . It is theoretically guaranteed that the position of the reflection base point  $O_{TM}$  remains stable during the rotation. The relative position of the reflection base point  $O_{TM}$  and the measurement base point  $O_B$  remains unchanged during the rotation.

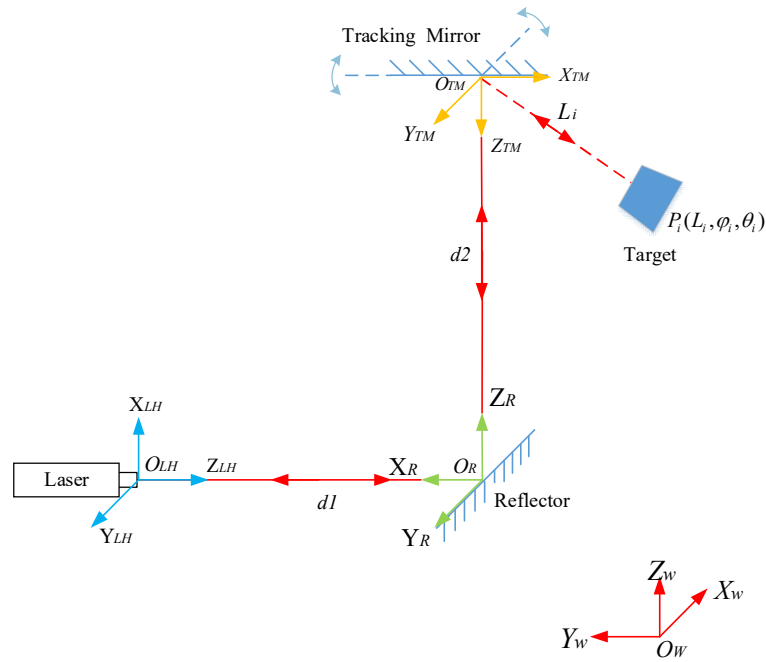


**Figure 2.** Mathematical model of laser tracking measurement system.

### 3. Materials and methods

#### 3.1. Measurement coordinate derivation

As shown in Figure 2, it is assumed that the origin  $OLH$  of the laser head coordinate system  $\{O_{LH}\}$  is represented as  $OLH(X_0, Y_0, Z_0)$  in the world reference coordinate system  $\{O_W\}$ , the distance between the point  $OLH$  and the point  $OR$  is represented as  $d1$  and the distance between the point  $OR$  and the point  $OTM$  is expressed as  $d2$ . The coordinate representation of a target point  $\{O_p : L_i, \phi_i, \theta_i\}$  in the measurement space coordinate system  $\{O_p\}$  has been derived in the world reference coordinate system  $\{O_W\}$ . According to the conversion relationship of the space coordinate system and the Cartesian coordinate system, the coordinates  $\{PTM : X_{TM}, Y_{TM}, Z_{TM}\}$  in the tracking mirror coordinate system  $\{O_{TM}\}$  of the target point  $\{O_p : L_i, \phi_i, \theta_i\}$  in the target spherical coordinate system  $\{O_p\}$  can be expressed as

$$\begin{cases} X_{TM} = L \sin \theta \cos \phi \\ Y_{TM} = L \sin \theta \sin \phi \\ Z_{TM} = L \cos \theta \end{cases} \quad (1)$$

where  $L$  is the absolute distance from the base point  $OB$  to the target point  $P_i$ .  $\theta$  and  $\phi$  are, respectively, the horizontal pitch angle and the vertical yaw angle of the tracking mirror.

The conversion process from the tracking mirror coordinate system  $\{O_{TM}\}$  to the mirror coordinate system  $\{O_R\}$  has the following stages.

1) Rotate the  $Z_{TM}$  axis in the coordinate system  $\{O_{TM}\}$  around the  $Y_R$  axis in the coordinate system  $\{O_R\}$  by  $180^\circ$  or  $-180^\circ$  (the counterclockwise direction is the positive direction of the rotating axis, and the clockwise direction is negative) so that the  $Z_{TM}$  axis coincides with the  $Z_R$  axis (the other two axes also coincide).

2) Move the coordinate system  $\{OTM\}$  along the  $ZR$  axis in the coordinate system  $\{OR\}$  by  $d_2$  distance in such a way that the two coordinate system origins  $OTM$  and  $OR$  coincide. At this time, the two coordinate systems coincide. The conversion matrix  $AR \leftarrow TM$  of the tracking mirror coordinate system  $\{OTM\}$  to the mirror coordinate system  $\{OR\}$  reads as follows:

$$AR \leftarrow TM = Trans(0,0,d_2)Rot(Z_{TM},180) \quad (2)$$

The conversion process from the mirror coordinate system  $\{OR\}$  to the laser head coordinate system  $\{OLH\}$  is as follows: first, the  $ZR$  axis is rotated by  $90^\circ$  around the  $YLH$ -axis (the direction of rotation is the same as the above steps) so that the  $ZR$ -axis and the  $ZLH$ -axis directions of the two coordinate systems coincide (the other two axes also coincide). Then, shift the coordinate system  $\{OR\}$  along the  $ZLH$  axis by  $d_1$  distance so that the two coordinate system origins  $OR$  and  $OLH$  coincide, and the two coordinate systems coincide. The transformation matrix  $ALH \leftarrow R$  of the mirror coordinate system  $\{OR\}$  to the laser head coordinate system  $\{OLH\}$  can be expressed as

$$ALH \leftarrow R = Trans(0,0,d_1)Rot(Z_R,90) \quad (3)$$

The conversion process from the laser head coordinate system  $\{OLH\}$  to the world reference coordinate system  $\{O_w\}$  is as follows: first, the  $ZLH$  axis is rotated by  $90^\circ$  around the  $X_w$  axis (the positive and negative rotation directions are the same as the above-mentioned directions) so that the  $ZLH$ -axis and the  $Z_w$ -axis directions coincide. Then, rotate the  $YLH$  axis by  $90^\circ$  around the  $Z_w$  axis (the positive and negative rotation directions are the same as above) so that the  $YLH$ -axis and the  $Y_w$ -axis directions coincide (the  $XLH$ -axis and the  $X_w$ -axis directions also coincide). Finally, the coordinate system  $\{OLH\}$  origin  $OLH$  is translated to the coordinate system  $\{O_w\}$  origin  $O_w$  so that the two coordinate system origins  $OLH$  and  $O_w$  coincide, and the two coordinate systems coincide. The conversion matrix  $AW \leftarrow LH$  of the laser head coordinate system  $\{OLH\}$  to the world reference coordinate system  $\{O_w\}$  can be expressed as

$$AW \leftarrow LH = Trans(X_0,Y_0,Z_0)Rot(Y_{LH},90)Rot(Z_{LH},90) \quad (4)$$

The conversion process for the tracking mirror coordinate system  $\{OTM\}$  to the world reference coordinate  $\{O_w\}$  can be obtained from Eqs (2)–(4), and the transformation matrix  $AW \leftarrow TM$  takes the following form:

$$AW \leftarrow TM = AW \leftarrow LH ALH \leftarrow R AR \leftarrow TM \quad (5)$$

In view of Eqs (2)–(4), we can calculate the rotation matrix  $R$  and the translation matrix  $S$  between the coordinate systems:

$$R_{R \leftarrow TM} = \begin{bmatrix} -1 & 0 & 0 \\ 0 & 1 & 0 \\ 0 & 0 & -1 \end{bmatrix}, S_{R \leftarrow TM} = \begin{bmatrix} 0 \\ 0 \\ d_2 \end{bmatrix} \quad (6)$$

$$R_{LH \leftarrow R} = \begin{bmatrix} 0 & 0 & 1 \\ 0 & 1 & 0 \\ -1 & 0 & 0 \end{bmatrix}, S_{LH \leftarrow R} = \begin{bmatrix} 0 \\ 0 \\ d_1 \end{bmatrix} \quad (7)$$

$$R_{W \leftarrow LH} = \begin{bmatrix} 0 & -1 & 0 \\ 0 & 0 & -1 \\ 1 & 0 & 0 \end{bmatrix}, S_{W \leftarrow LH} = \begin{bmatrix} X_0 \\ Y_0 \\ Z_0 \end{bmatrix} \quad (8)$$

According to the conversion relationship between the coordinate systems [18], it can be known that the relationships between the tracking mirror coordinate system  $\{OTM\}$ , each intermediate coordinate system and the world reference coordinate system  $\{O_W\}$  can be expressed as follows:

$$P_R = R_{R \leftarrow TM} P_{TM} + S_{R \leftarrow TM} \quad (9)$$

$$P_{LH} = R_{LH \leftarrow R} P_R + S_{LH \leftarrow R} \quad (10)$$

$$P_W = R_{W \leftarrow LH} P_{LH} + S_{W \leftarrow LH} \quad (11)$$

By substituting Eqs (6)–(8) into Eqs (9)–(11), the coordinate representations in the tracking mirror coordinate system  $\{OTM\}$   $\{PTM:XTM, YTM, ZTM\}$  in each intermediate coordinate system and the world reference coordinate system  $\{O_W\}$  can be expressed as

$$\begin{aligned} P_R &= [X_R, Y_R, Z_R]^T \\ &= [-X_{TM}, Y_{TM}, -Z_{TM} + d_2]^T \end{aligned} \quad (12)$$

$$\begin{aligned} P_{LH} &= [X_{LH}, Y_{LH}, Z_{LH}]^T \\ &= [-Z_{TM} + d_2, Y_{TM}, X_{TM} + d_1]^T \end{aligned} \quad (13)$$

$$\begin{aligned} P_W &= [X_W, Y_W, Z_W]^T \\ &= [X_{TM} + d_1 + X_0, Z_{TM} - d_2 + Y_0, -Y_{TM} + Z_0]^T \end{aligned} \quad (14)$$

Combining Eqs (1) and (14), the target point in the target space coordinate system  $\{O_P\}$  is  $\{O_P: L_i, \varphi_i, \theta_i\}$ . Its coordinate  $\{P_W: X_W, Y_W, Z_W\}$  in the world reference coordinate system  $\{O_W\}$  is expressed as follows:

$$\begin{cases} X_W = L \sin \theta \cos \varphi + d_1 + X_0 \\ Y_W = L \cos \theta - d_2 + Y_0 \\ Z_W = -L \sin \theta \sin \varphi + Z_0 \end{cases} \quad (15)$$

Here,  $L$  represents the absolute distance from the measurement base point  $O_B$  to the target point  $O_P$ .  $L$  is determined from the known reference distance  $L_B$ , which must be calibrated before the measurement. The tracking mirror horizontal pitch angle  $\theta$  and the vertical yaw angle  $\varphi$  are respectively given by corresponding grating reading systems.  $d_1$  and  $d_2$  and the coordinates  $(X_0, Y_0, Z_0)$  are system parameters that have been determined before measurement.

#### 4. Measurement principle

Based on the distance measurement principle of the Michelson interferometer, according to the interference signal generated by the reflected light and the reference light on the surface of the detector, the number of interference fringe changes is calculated to obtain the displacement of the target, and the tracking and ranging of the target is realized. The beam emitted by the rotating laser is split into two beams by the polarizing beam-splitting prism. One of the two beams returns from the original path

after reflection of the corner cube reflector as the reference beam. Another beam (the probe) goes through the tracking mirror to the cat's eye retroreflector at the target point.

After collecting the position information on the measured target point, the measurement beam returns from the original way and interferes with the reference beam to obtain the amount of change in the length of the measured target point and the measurement base point. Figure 3 shows a schematic diagram of the laser tracking measurement system via the stereo coordinate system method.

The returned measurement beam is split by the beam-splitting prism and directed toward the PSD (photoelectric position-detecting device) to detect the positional change of the cat's eye retroreflector. When the cat's eye retro mirror moves, the position of the spot on the PSD changes. The signal acquisition processing circuit detects this change and sends the change information to the tracking control circuit. The tracking control circuit adjusts its speed by adjusting the voltage input to the servo motor to rotate the tracking mirror through a certain angle, thereby automatically adjusting the projection direction of the measurement beam so that it is always aligned with the cat's eye retroreflector. The yaw angle in the horizontal direction of the tracking mirror and the pitch angle in the vertical direction are respectively detected by the optical grating ruler mounted on the two motor shafts.

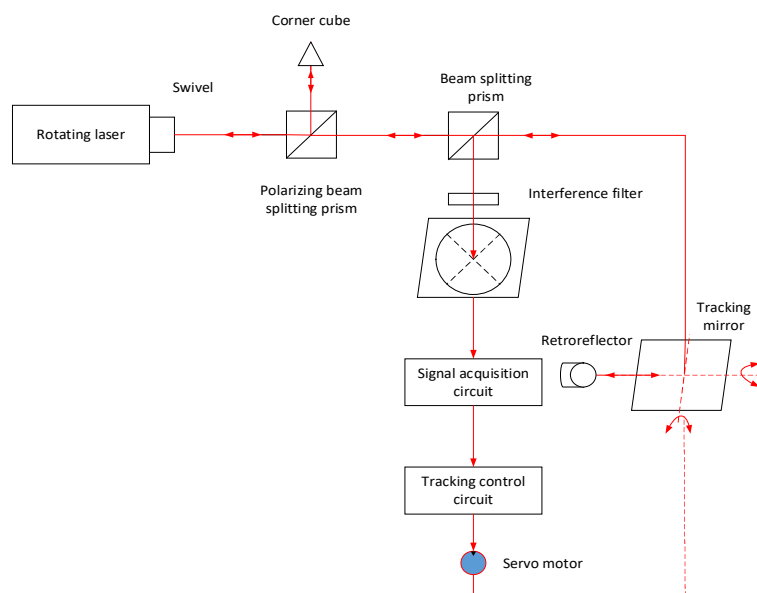


**Figure 3.** System measurement schematic.

## 5. System design

### 5.1. Interference light path for length detection

In order to obtain the position change of the target mirror, a splitting prism is used to split the returned measurement beam. A conventional beam-splitter plate has a typical thickness of 3 mm. The beam is reflected on both its front and back surfaces, producing two close-spaced spots (about 2.27 mm apart), one of which is the spot to be tested, as shown in Figure 4. The two spots may simultaneously enter the photosensitive surface of the PSD so that the position of the spot detected by the PSD is different from the actual position of the spot to be tested, causing an incorrect sensing signal. The use of a beam-splitting prism avoids the generation of double reflection spots.

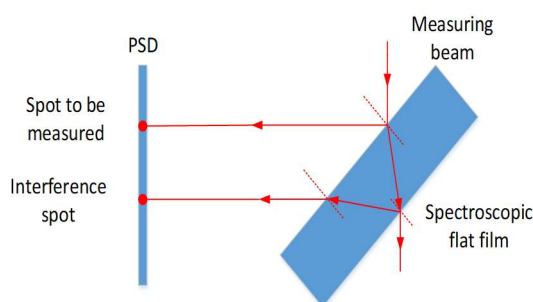


**Figure 4.** Double reflection spot of ordinary spectroscopic film.

Another aspect, which this study tackles, is the influence of external stray light on the shape of the PSD spot. In this respect, certain treatment measures must be considered. An effective treatment method is to add components, such as interference filters and mechanical sleeves. Thus, the laser beam entering the PSD is almost immune to external stray light. After the above-mentioned processing, the spot shape on the PSD was a very regular circle. The detected spot motion accurately reflects the motion of the target and ensures smooth tracking.

### 3.2. Target tracking process of photoelectric position sensor

The target-tracking test system using the PSD photoelectric position sensor is shown in Figure 5. The whole system is a rough and precise double closed-loop tracking structure [19,20]. Among them, the coarse tracking system with a PSD as the main sensor completes the pointing function of the initial target. The fine tracking system uses a CMOS camera as the main sensor to perform precise position feedback. The purpose of the final tracking is to complete real-time alignment function between the motion beacon and the fixed tracking system. The calibration of the moving position of the beacon is obtained through real time data capture via GPS receiver carried by the moving target when the range of motion is large and the distance is long.

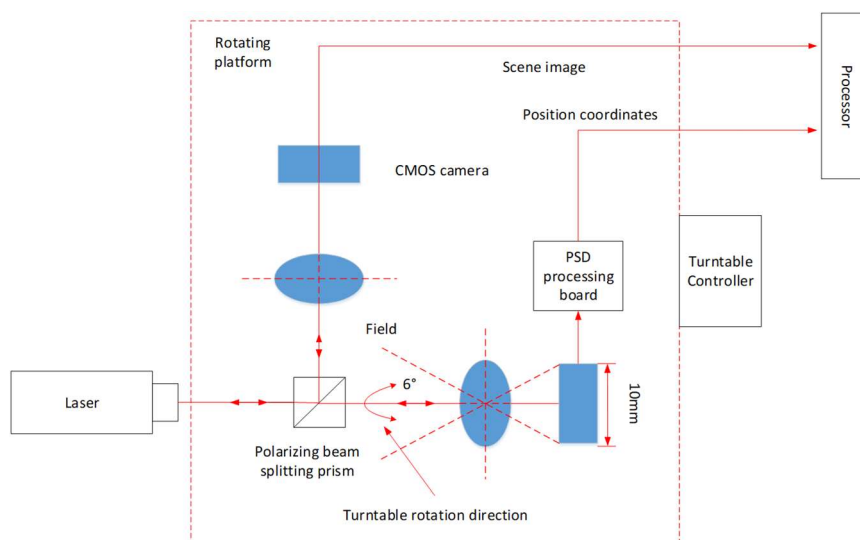


**Figure 5.** Schematic representation of the PSD photoelectric position tracking system.

Regarding the system shown in Figure 5, it consists mainly of a PSD measurement optical path,

a CMOS imaging optical path, a one-dimensional turntable and a beacon system. Among them, the PSD measurement optical path realizes the coarse tracking function; the PSD sensor was an S5991-01 from Hamamatsu of Japan; the nominal position error was  $\pm 0.15$  mm, and the resolution was  $\pm 1.5$   $\mu\text{m}$ . The CMOS imaging optical path completes the fine tracking function. The experiment was carried out with a BFLY-PGE-13E4C camera, which had a cell size of  $5.3$   $\mu\text{m}$ , pixel size of  $1280 \times 1024$  and refresh rate of (60 frames/s). The one-dimensional tracking turntable realizes the target tracking function and completes the real-time output function of the following position (only considering the azimuth direction). The rotation range was  $360^\circ$ , the step accuracy was  $0.015^\circ$ , the highest angular velocity was  $10^\circ/\text{s}$  and the angular acceleration was  $2^\circ/\text{s}^2$ . The focal length of the PSD front lens in the system was 50 mm. The optical path structure of the test host and beacon light hitting the PSD target surface is shown in Figure 6.

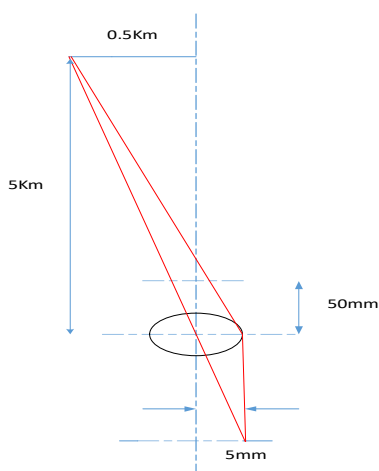


**Figure 6.** PSD target surface optical path structure equivalent position optical path diagram.

After the beacon light enters the PSD observation field of view ( $\pm 6^\circ$ ), the position of the beacon light image projected onto the PSD surface is calculated using the optical imaging relationship. The spot detected by the PSD photosensitive surface changes in displacement, and the position information is solved in the controller through data acquisition. The target horizontal (or pitch) position information is obtained and passed to the one-dimensional tracking turntable, deflecting the tracking mirror by a certain angle and adjusting the direction of the measurement beam until the spot offset detected by the PSD is 0 to complete coarse tracking pointing of the system. By coarse tracking pointing, it is ensured that the beacon light can fall into the CMOS fine tracking field of view ( $\pm 1^\circ$ ) for a more accurate tracking process. In this process, the PSD sensor's fast position acquisition capability and high-speed dynamic response characteristics are fully utilized. After filtering, the output stable and accurate position information is used for the subsequent fine tracking process.

## 6. Experiment

### 6.1. PSD position detection and nonlinear correction

First, we set up an optical path to measure the fixed point and repeated the measurement for each point 100 times (0.004~0.4 ms, sampling once every 0.004 ms; here, 20 sets of data were taken), obtaining its  $X$  and  $Y$  coordinate values and corresponding voltage values. We then fit the test data for

the fixed point in the  $X$  and  $Y$  directions, as shown in Figure 7. It can be seen from the figure that the  $X$  and  $Y$  coordinates were unstable due to the existence of some external factors and internal factors of the PSD, such as the irregular shape of the PSD detector electrode, the uneven distribution of the junction resistance in the P zone, the nonlinearity of the PSD caused by interference light in the laboratory and temperature drift.

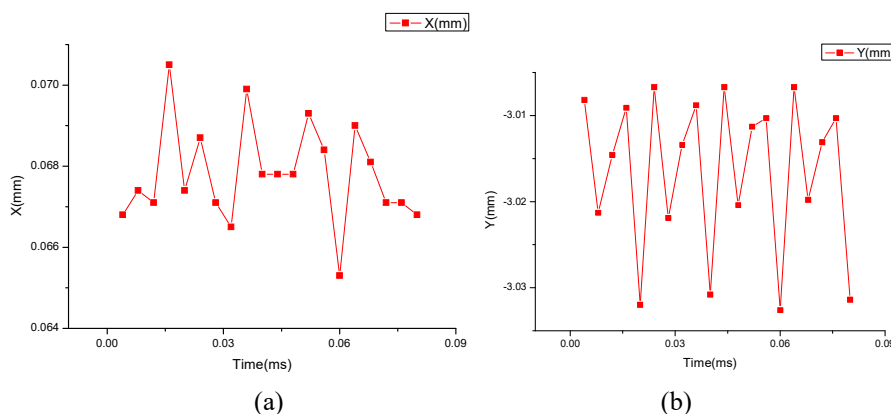


**Figure 7.** Fixed point  $XY$  test data fitting. (a)  $X$  direction test data fitting; (b)  $Y$  direction test data fitting.

The ideal PSD device has a good linear relationship between the output current value and the spot-center coordinate value. Due to the influence of background light, external noise and uneven distribution of its own surface resistance, the output of PSD devices often has errors, so an effective means is needed to solve the PSD nonlinearity problem. There are many correction methods for PSDs, such as neural network algorithms, linear interpolation methods, conjugate gradient algorithms, etc. This study uses a Bayesian regularization L-MBP (Levenberg-Marquardt) algorithm to correct the nonlinearity of the PSD. According to the measurement principle, we built a measurement system, analyzed the measured value and performed the steps mentioned in the previous section to complete the nonlinear correction of the PSD measurement system. The measuring experimental device is shown in Figure 8. The method developed in this study involves the following experimental steps:

(1) Control the three-dimensional CNC (computerised numerical control machine) module to make the laser beam pass through the filter and establish a coarse focus on the geometric center of the PSD photosensitive surface;

(2) By adjusting the precision  $XY$  stage, adjust the position of the PSD photosensitive surface for fine focus until the coordinates are displayed (0.000x, 0.000y) (mm). Here, because the vibration of the platform cannot be avoided during the experimental operation, the coordinates were accurate to 1  $\mu\text{m}$  during data collection, which also means that  $x$  and  $y$  were between 0–5 mm;

(3) Control the three-dimensional CNC module, adjust the position of the laser beam and scan the PSD photosensitive surface in a “back” shape with a step length of 1 mm, as shown in Figure 9. At the same time, the coordinate points should be sampled and recorded at a sampling frequency of 100 Hz;

(4) Process the PSD location information data set and train the neural network model with the Bayesian regularized L-MBP algorithm;

(5) Train the neural network model, use the model to apply the nonlinear correction to the PSD and analyze the experimental results.

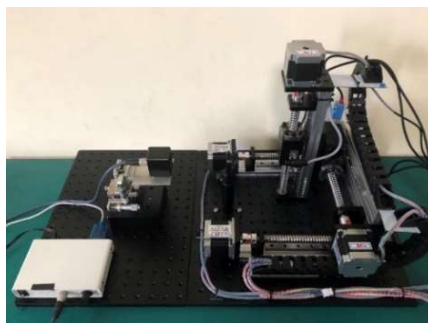


**Figure 8.** PSD nonlinear measurement device.

The PSD nonlinear correction experiment used FUYU's FSL40XYZ-L three-dimensional CNC module as the platform, and the test used the C10443-02 two-dimensional quadrilateral PSD and C10443 signal processing system. The effective photosensitive area of the PSD was  $9\text{ mm} \times 9\text{ mm}$ ; the spectral response was 320–1100 nm, the peak sensitivity wavelength was 960 nm, the saturated incident light power was  $167\ \mu\text{W}$ ; the resolution was  $150\ \mu\text{m}$ ; the laboratory laser light source was a spot laser with a wavelength of 850 nm and a power of 1 mW. The laser transmitter was fixed on the three-dimensional CNC module.

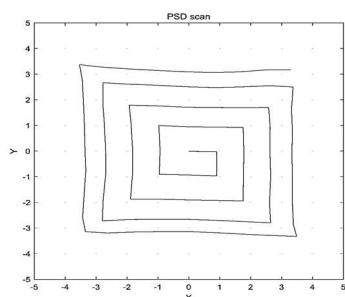


**Figure 9.** “Back” scanning PSD photosensitive surface.

In order to reduce the power of the light source to the measurable range, the output power of the light source was reduced by the filter.

Figure 10 shows the results of the test and the results after linear correction.

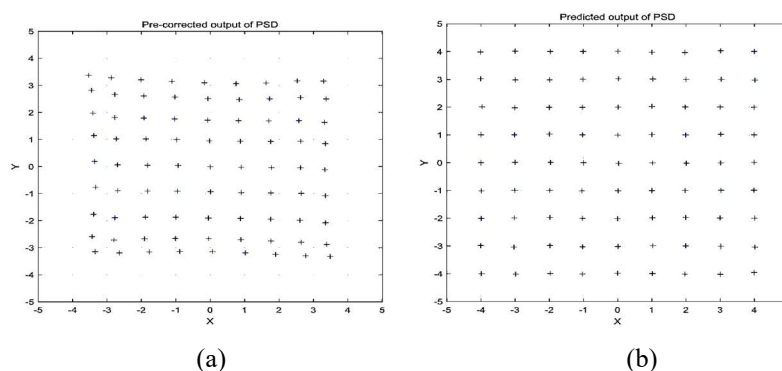


**Figure 10.** Test result without linear correction and the result after linear correction. (a) Location data when not optimized; (b) Optimized location data.

It follows from Figure 10 that the test results after the Bayesian regularization correction method were obviously biased toward linearization in the edge area. Before the correction, the distribution of points was more scattered. Compared with that before the correction, the result after the correction had a smaller error and higher accuracy. The data display accuracy reached 0.2  $\mu\text{m}$ .

## 6.2. Experimental setup of 3D laser tracking system

By Using the STM32 serial port to communicate with the PC serial debugging assistant, controlling a stepper motor drive can realize relative position movement and absolute position movement. One can set the number of sent pulses (position), the pulse frequency (speed) and the rotation direction. Here, we employed 20 hollow shaft stepping motors with 8- and 5-mm couplings. The rotating laser scanner is depicted in Figure 11.



**Figure 11.** Photograph of the rotating laser scanner.

We placed the rotating laser very close to the front of the PSD and adjusted the two-dimensional displacement platform to position the PSD at the (0,0) point. Then, we rotated the laser one circle clockwise in 0.5-mm steps to capture the PSD output value of 25 points with the PSD light surface in the range of 1  $\text{mm}^2$ . When the laser rotated at each collection point, the output voltage of the PSD electrode was mapped to the incident light intensity. Figure 12 below shows the least-squares circle fitting for each trajectory.

As it can be seen in Figure 12, the circle is the center of gravity of the laser rotation and the circumference was the movement of the spot position (the position of the center of gravity of the spot measured by the PSD). When the beam emitted by the rotating laser was reflected by the mirror to the tracking mirror, it was then emitted from the tracking mirror to the target mirror. The target was fixed on the spindle of the CMM and moved along with the CMM spindle. When the CMM spindle moved, the tracking mechanism changed the direction of the laser beam exiting so that the beam always pointed toward the center of the target. After many experimental tests, the system achieved stable tracking when the cat's eye retroreflector moved in the X, Y and Z directions at a speed of 0.2 m/s within the range of 1800  $\text{mm} \times 4000 \text{ mm} \times 1200 \text{ mm}$ . The tracking speed of 0.4 m/s was achieved within the range of 1~2 m; consequently, the tracking effect was better.

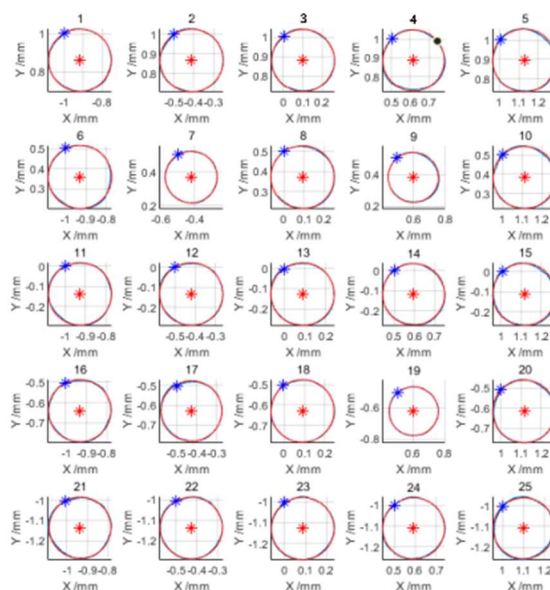


**Figure 12.** Spatial distribution of the rotating laser PSD output.

## 7. Conclusions

The rotating laser tracking measurement is based on the space coordinate method, where the actual structure and optical path of the space coordinate laser tracking measurement system. In this study, we developed the ideal mathematical model of the system and the coordinate expression of any measured point in the world reference coordinate system. We achieved further optimization of the laser tracking mechanism and improvement of the tracking control system. Our system ensures the reliability of tracking and good static and dynamic characteristics. A Bayesian regularized L-MBP algorithm was used to solve the PSD nonlinearity problem. The output response of the PSD to the laser rotation and the linearity of the sensing position signal of the detection circuit were analyzed. The target mirror was installed on the CMM measuring spindle to test the tracking ability of the system. The laser tracking measurement system established by this measurement method satisfies the new requirements of large-scale, high-precision, flexible measurement without rails, on-site measurement and dynamic real-time tracking measurement. This has become an irreplaceable measurement tool in many fields, and it has very broad application prospects. In the future, we may advance to research stochastic prediction of PSDs [21,22].

## Acknowledgments

This research was funded by the Shanghai Science and Technology Innovation Action Plan, grant numbers 22S31903700, 21S31904200, National Natural Science Foundation of China (NSFC), grant number U1831133 and Natural Science Foundation of Shanghai, grant number 17ZR1443500.

## Conflict of interest

The authors declare that there is no conflict of interest.

## References

1. Y. Y. Yin, Y. M. Guo, A study on the measurement coordinate system of various large-scale measuring instruments, *Metrol. Meas. Technol.*, **36** (2016), 10–15.
2. H. Noura, J. P. Wallerand, M. Malak, A. F. Obaton, J. Salgado, T. Bourouina, Miniature silicon Michelson interferometer characterization for dimensional metrology, *Sensors Actuators A Phys.*, **223** (2015), 141–150. <https://doi.org/10.1016/j.sna.2014.12.031>
3. Q. X. Lu, X. H. Lu, Design of robot laser global positioning system based on dynamic tracking measurement, *Laser J.*, **40** (2019), 188–191.
4. X. D. Zhang, K. Bu, Y. W. Dong, X. J. Li, Fast and precise positioning method for three-coordinate measurement of complex curved surface parts based on iterative algorithm, *J. Aerosp. Power*, **33** (2018), 2525–2532. <https://doi.org/10.13224/j.cnki.jasp.2018.10.026>
5. Z. L. Yang, Y. S. Chen, X. G. San, Y. H. Zhang, Z. Y. Wu, Design of data acquisition and transmission system for spot detection of four quadrant detectors, *LCD Disp.*, **31** (2016), 80–86. <https://doi.org/10.3788/YJYXS20163101.0080>
6. Y. J. Peng, L. H. Li, X. S. Tang, R. Gao, Response characteristics of position sensitive detector under oblique incidence condition, *Semicond. Photonics Technol.*, **15** (2009), 56–74.
7. M. H. Jun, Y. M. Kim, Accuracy evaluation of robotic tonometry pulse sensor system based on radial artery pulse wave simulator, *IEEE Trans. Instrum. Meas.*, **69** (2020), 7646–7657. <https://doi.org/10.1109/TIM.2020.2981107>
8. E. Shim, Y. Kim, D. Lee, B. H. Lee, S. Woo, K. Lee, 2D-3D registration for 3D analysis of lower limb alignment in a weight-bearing condition, *Appl. Math.*, **33** (2018), 59–70. <https://doi.org/10.1007/s11766-018-3459-2>
9. X. M. Garcia-Cruz, O. Y. Sergiyenko, V. Tyrsa, M. Rivas-Lopez, D. Hernandez-Balbuena, J. C. Rodríguez-Quiñonez, et al., Optimization of 3D laser scanning speed by use of combined variable step, *Optics Lasers Eng.*, **54** (2014), 141–151. <https://doi.org/10.1016/j.optlaseng.2013.08.011>
10. J. C. Rodríguez-Quiñonez, O. Sergiyenko, W. Flores-Fuentes, M. Rivas-lopez, D. Hernandez-Balbuena, R. Rascón, et al., Improve a 3D distance measurement accuracy in stereo vision systems using optimization methods' approach, *Opto-Electronics Rev.*, **25** (2017), 24–32. <https://doi.org/10.1016/j.opelre.2017.03.001>
11. L. Lindner, O. Sergiyenko, J. C. Rodríguez-Quiñonez, V. Tyrsa, P. Mercorelli, W. F. Fuentes, et al., Continuous 3D scanning mode using servomotors instead of stepping motors in dynamic laser triangulation, in *2015 IEEE 24th International Symposium on Industrial Electronics (ISIE)*, (2015), 944–949. <https://doi.org/10.1109/ISIE.2015.7281598>
12. C. Bányász, L. Keviczky, R. Bars, How to teach control system optimization (a practical decomposition approach for the optimization of TDOF control systems), *IFAC PapersOnLine*, **52** (2019), 115–120. <https://doi.org/10.1016/j.ifacol.2019.08.134>
13. K. N. Song, B. Wang, C. Y. Tang, Research on indoor positioning method based on laser ranging scan, *Laser Infrared*, **46** (2016), 938–942. <https://doi.org/10.3969/j.issn.1001-5078.2016.08.006>
14. A. Gleadall, N. Vladov, J. Segal, S. Ratchev, M. Plasch, D. Kimmig, et al., A decision support methodology for embodiment design and process chain selection for hybrid manufacturing platforms, *Int. J. Adv. Manuf. Technol.*, **87** (2016), 553–569. <https://doi.org/10.1007/s00170-016-8514-7>

15. F. G. Galizia, H. ElMaraghy, M. Bortolini, C. Mora, Product platforms design, selection and customisation in high-variety manufacturing, *Int. J. Prod. Res.*, **58** (2020), 893–911. <https://doi.org/10.1080/00207543.2019.1602745>
16. W. L. Liu, X. H. Qu, J. F. Ouyang, Modeling and simulation of laser tracking measurement system, *J. Petrochem. Univ.*, **20** (2007), 50–53. <https://doi.org/10.1108/03684921211275207>
17. J. K. Jang, S. H. Abbas, J. R. Lee, Investigation of underwater environmental effects in rotating propeller blade tracking laser vibrometric measurement, *Optics Laser Technol.*, **132** (2020), 106460. <https://doi.org/10.1016/j.optlastec.2020.106460>
18. G. Guo, J. Han, J. Lv, J. Mu, L. Guo, L. Y. Li, Experimental study on the influence of three-coordinate touch direction on measurement accuracy, *Aerosp. Manuf. Technol.*, **6** (2015), 18–20.
19. A. Formato, D. Guida, D. Ianniello, F. Vilecco, T. L. Lenza, Pellegrino, A design of delivery valve for hydraulic pumps, *Machines*, **6** (2018), 44. <https://doi.org/10.3390/machines6040044>
20. S. Xiao, X. Ge, Q. L. Han, Y. Zhang, Z. Cao, Distributed guaranteed two-target tracking over heterogeneous sensor networks under bounded noises and adversarial attacks, *Inf. Sci.*, **535** (2020), 187–203. <https://doi.org/10.3390/machines6040044>
21. W. Q. Song, L. He, Z. Enrico, Long-range dependence and heavy tail characteristics for remaining useful life prediction in rolling bearing degradation, *Appl. Math. Modell.*, **102** (2022), 268–284. <https://doi.org/10.1016/j.apm.2021.09.041>
22. S. Duan, W. Q. Song, E. Zio, C. Cattani, M. Li, Product technical life prediction based on multi-modes and fractional Lévy stable motion, *Mech. Syst. Signal Process.*, **161** (2021), 107974. <https://doi.org/10.1016/j.ymsp.2021.107974>



AIMS Press

©2023 the Author(s), licensee AIMS Press. This is an open access article distributed under the terms of the Creative Commons Attribution License (<http://creativecommons.org/licenses/by/4.0>)